Springer

KSME

Journal of Mechanical Science and Technology 32 (4) (2018) 1705~1711
www.springerlink.com/content/1738-494x(Print)/1976-3824(Online)
DOI 10.1007/s12206-018-0327-1

CFD analysis of effects on fluid flow resistance of metallic wavy structures †

Jeong-Ho Yang[1] and Sang-Hu Park[2,*]
[1]*Graduate School of Mechanical Engineering, Pusan National University, Busan 609-735, Korea*
[2]*School of Mechanical Engineering and ERC/NSDM, Pusan National University, Busan 609-735, Korea*

(Manuscript Received October 7, 2017; Revised December 17, 2017; Accepted January 14, 2018)

Abstract

Microscale wrinkles can be utilized to enhance the characteristics of products. For example, a shark skin having riblet surface can move faster underwater, minimizing fluid flow resistance. We introduce a novel approach to fabricate microscale metallic wrinkles using a soft lithography and electroforming process; we also evaluated the effects of wrinkles by computational fluid dynamics (CFD) analyses. For the generation of metallic wrinkles, a UV-curable resin, NOA68T was used to fabricate a master wrinkling pattern by mechanism of compressive forces on a skin of the weakly polymerized resin layer. The master pattern was molded and replicated as metallic wrinkles on a surface via soft lithography and electroforming processes. To understand the advantages of a wavy surface on reduction of flow resistance, we carried out two- and three-dimensional (2D and 3D) CFD analyses. The drag coefficient of a wrinkled 2D square model was decreased about 17.1 %, and a 3D real wrinkle model showed 4.9 to 7.3 % reduction of it compared to without wrinkle models. We believe that it is possible to reduce the fluid flow resistance using wavy surfaces that can easily be generated selectively or wholly on an arbitrary surface.

Keywords: Microscale metallic wrinkles; PDMS molding; Weak polymerization; Drag coefficient; Flow resistance; CFD

1. Introduction

Various types of microscale surface wrinkles exist in nature for special functions; they can often be observed in the skin of animals and plants that have inherent characteristics. Riblet-shaped denticles on a shark skin enable to move faster underwater; humpback whale fins assist to increase driving force during underwater movement; and the skin wrinkle of a snake is shaped to reduce friction [1-3]. Also, wrinkles have various characteristics of increasing the heat transfer efficiency, superhydrophobic surfaces, and others [4-7].

Till now, a number of research reports have been introduced to fabricate and mimic wrinkling surfaces. These include reports to control the width and height of microscale wrinkle structures by exposing ultraviolet (UV) light on the coated photocurable resin [8]. In addition, microscale hierarchical wrinkles were fabricated by repeatedly dividing the volume of a resin layer using UV light and plasma treatment [9]. Also, some effective ways were reported: a method to use temperature variation on a metal-ion-coated polymer surface to generate wrinkles [10]; a wrinkling method using UV light exposure and water swelling on a polyhydroxyethyl methacrylate (PHEMA) film, and a method of controlling the height of the wrinkles by exposure to an ion beam [11, 12].

Replicative methods using soft lithography have been introduced. Micro-and-nanoscale wrinkles were replicated using polydimethylsiloxane (PDMS) [13]. Microscale wrinkle patterns with hierarchical structures by pre-tensile strain and plasma exposure were generated [14]. Others for wrinkling have been reported [15-17]. A few research works related to the effects of microscale wrinkles have been reported. Numerical analyses of shark skin using computational fluid dynamics (CFD) to understand the drag reduction, and analytical study on the effects of fluid flow on the turbine-blade mimicking humpback whale fins were reported [18, 19]. Also, the mechanism of drag reduction and characteristics of flow resistance on dimple effect were introduced [20-23].

However, there are still issues to be settled down for a wide use of wrinkling structures in industry. For example, there are few reports on fabrication of metallic wrinkles. Metallic wrinkle has some advantages like high heat transfer efficiency, high mechanical strength and durability. Therefore, in this work, we analyzed two- and three-dimensional (2D and 3D) wrinkling models, of which size and shape obtained from a real metallic wrinkling process, using CFD in order to know the effects of surface wrinkles on fluid flow resistance and further applications.

*Corresponding author. Tel.: +82 51 510 1011, Fax.: +82 51 513 4305
E-mail address: sanghu@pusan.ac.kr
† Recommended by Associate Editor Suk Goo Yoon

2. Generation of metallic wrinkles

We utilized a soft PDMS mold to replicate metallic wrinkles from a polymeric mater wrinkle pattern. A NOA68T (Norland Co., Germany) resin was mainly used to generate microscale master wrinkles. The resin undergoes fully photo-induced polymerization by exposure of UV light of 4.5 J/cm^2. NOA68T resin has high affinity with other materials, low toxicity to the human body, and is widely used as a photo curing adhesive. PDMS was mainly used to fabricate the master mold. The PDMS mold was obtained by mixing sylgard 184-a and curing agent, sylgard 184-b (Dow Corning, U.S.A.).

As the first step, the microscale wrinkle master was fabricated. As depicted in Fig. 1(a), NOA68T resin was coated on the substrate with a thin layer thickness of approximately 150 μm, and then shortly exposed to UV light for 15 sec in order to get weak polymerization on the layer. A relatively strong polymerization reaction occurs on the skin of layer, and a weak polymerization occurs under the skin (inside of layer). The difference in the relative density of polymerization between the skin layer and the inside layer resulted in a material property gradient in the direction of the layer thickness. After that, a thermal curing proceeded under room temperature of 30 ℃ for three hours to be perfectly cured. During this process, a compressive force (f_c) was generated on the skin owing to volume shrinkage of the layer. Previous works show that the wrinkle shapes can be controlled by the layer thickness of resin [8]. Also, the wrinkling wavelength (λ) is dependent on electricity modulus of skin (E_s) and inside (E_i) as expressed; $\lambda \sim (E_s/E_i)^{1/3}$ [24]. And then, a soft PDMS mold was fabricated using the master wrinkles, and sputtered to cover a gold seed layer on the surface using a sputter coater (Q150R, Quorum Technologies, U.K.) for the next metallic replication step described the below section.

To fabricate the metallic wrinkle, a nickel electroforming method was utilized as shown in Fig. 1(b). A nickel electrolyte was prepared by mixing 600 g/L of a sulfamic acid solution, 30 g/L of boric acid, and 5 g/L of nickel chloride in an electroforming tank [25-27]. This nickel electrolyte has high solubility and can be used at high density and current. As shown in Fig. 1(b), the ion-coated PDMS and the substrate were attached to the cathode plate of the electroplating tank, and then electric current connected. An electrical tape was connected between the two objects to flow current. In addition, a space (0.5 mm) in which an electrolyte could flow was made between the two objects. A nickel electroforming was performed for 8 hr.

The fabricated metallic wrinkles are shown in Fig. 2. The measurements of wrinkle line-width were taken at six points around a position and averaged. As shown in Fig. 2, the average widths of the master wrinkles were measured as 223 to 232 and 582 to 592 μm which were fabricated under different layer thickness of resin as 150 and 300 μm. Also, the average widths of replicated metallic wrinkles were measured as 228 to 231 and 585 to 592 μm, respectively. The shape and size was well matched between master wrinkle and replicated metallic one.

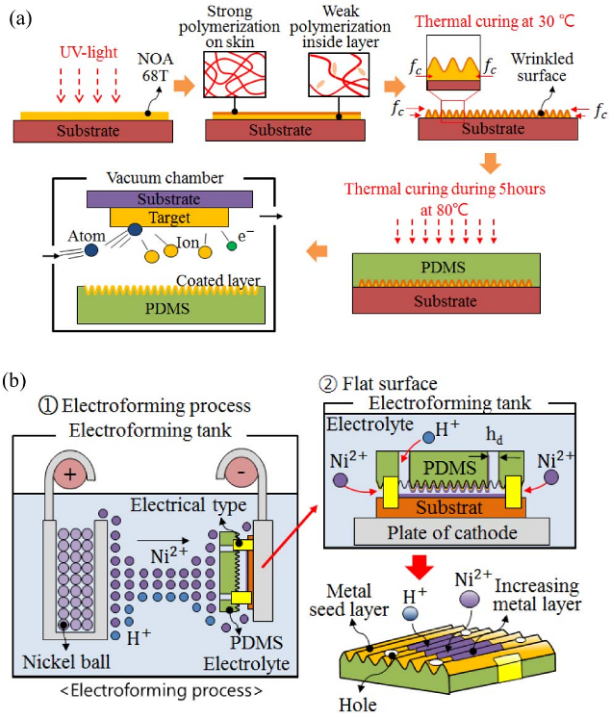

Fig. 1. Schematic processes of replication of metallic wrinkles: (a) Fabrication process of wrinkle master patterns: Weak polymerization and thermal curing process for master wrinkle generation weak polymerization and thermal curing process for master wrinkle generation and sputtering for metal seed layer on the mold; (b) schematic of electroforming process (①), the fabrication process of metallic wrinkles using the electroforming on a surface (②).

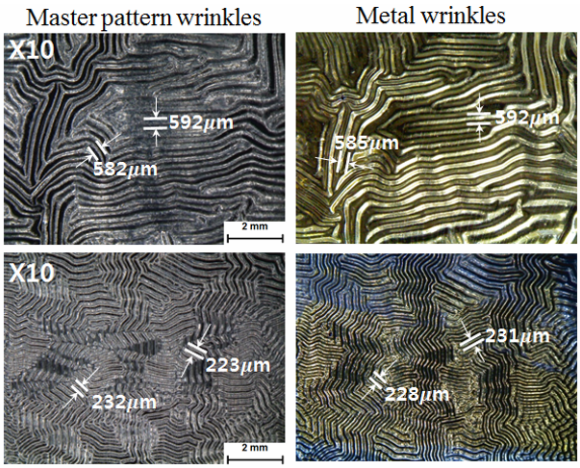

Fig. 2. Microscopic images of master and replicated metallic wrinkles.

3. Effects on reducing fluid flow resistance

3.1 Simple 2D wrinkled square model

A number of research works have done on drag coefficients using CFD and experiments. From the studies, we know that a dimple shape enables us to reduce the drag coefficient [25, 26].

Based on the idea, we tried to understand the effects of fluid flow resistance on surface wrinkles using a basic analysis model. Microscale wrinkles were simply modeled on the edge lines of a square. A CFD analysis was performed using the commercial code, Fluent (ver. 13, ANSYS, U.S.A.) with the Smagorinsky type of large eddy simulation (LES) model. CFD analysis was used to confirm the drag coefficient that influences fluid flow characteristics.

The drag coefficient is measured by the shear stress and pressure on a moving object in a fluid. The drag coefficient is expressed by Eq. (1). The drag force, which reacts in the x-direction, is expressed by Eq. (2):

$$C_d = \frac{F_d}{1/2\rho U^2 A} \quad (1)$$

$$F_d = \int p\cos\theta \, dA + \int \tau_w \sin\theta \, dA \quad (2)$$

where C_d is the drag coefficient, F_d is the drag force, ρ is the density of water, U is the inflow velocity, A is the area projected, p is the pressure, and τ_w is the shear stress. The low drag coefficient was effective to faster move in the fluid. We analyzed the method that can effectively reduce the fluid flow resistance by using a drag coefficient equation.

As shown in Fig. 3(a), the flow field was modeled by the inlet boundary condition of the 5 m/s velocity and the outlet boundary condition of 0 Pa pressure. In addition, the size of the flow field was 400×700 (height×width) mm. The fluid was applied to water at 25 ℃. As shown in Figs. 3(b) and (c), the shape parameters were analyzed by dividing them into two types: square with and without surface wrinkles. Each square length was modeled with a constant 10 mm. The shape of wrinkle was simplified as a semicircle with a width of 0.6 mm, which is the maximum size we can make. CFD analysis was carried out at Reynolds number (Re) of 20000.

Firstly, we checked the grid dependency of the model. Figs. 4(a)-(c) show mesh distribution of two models and test results of grid dependency. The grid number converged at the 16×10^4 element number. Also, the drag coefficient for each shape was 2.04 for a flat square, 1.69 for a square with wrinkles. The shape of the square with wrinkles reduced the flow resistance about 17.1 % compared to the square shape without wrinkles (see Figs. 5(a)-(c)). The width and height of wake portion on surface with wrinkle were reduced about 25.14 % more than flat surface due to a wrinkling effect.

To understand the change of wrinkling surface effect, we rotated the square to be a rhombus shape. The CFD analysis conditions were the same as previously described. As shown in Figs. 6(a) and (b), the drag coefficient of the wrinkled model was reduced about 10.1 % compared to the flat model.

Also, the height of wake was dramatically reduced as 42.6 % in case of the wrinkled model. The narrow zone of a wake enables to decrease the amount of pressure difference, so a drag force also reduced. By this mechanism, the flow resistance can be minimized when a wrinkling surface is applied [20]. From these results, we know that the wrinkling surface is quite effective to reduce flow resistance, and the reduction amounts are different depending on the shape of an object even though the same wrinkles are applied on its surface.

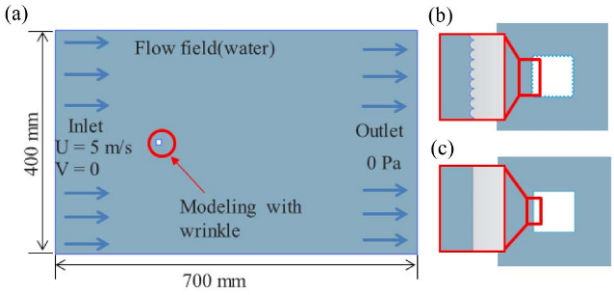

Fig. 3. Schematic boundary conditions of CFD: (a) Boundary condition of fluid field domain; (b) modeling of square shape with wrinkle width of 0.6 mm; (c) square shape without wrinkles.

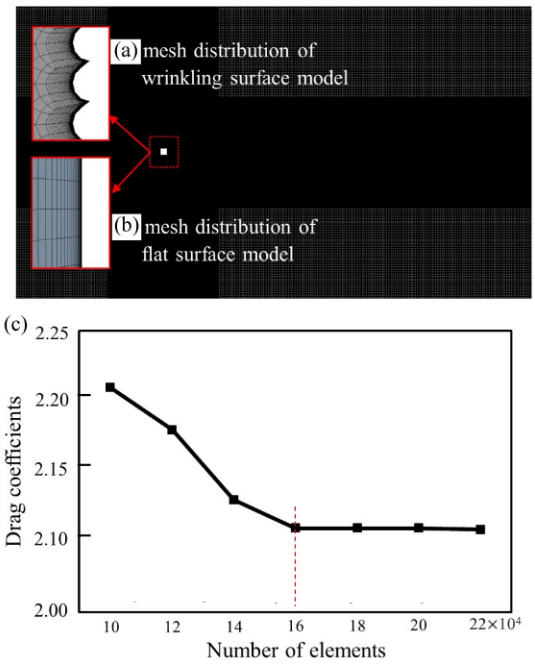

Fig. 4. (a) and (b) Mesh distribution of two models; (c) grid dependency test result.

We evaluated the variation of a drag coefficient according to locations of wrinkled surface in a square model. As shown in Fig. 7, a drag coefficient was more reduced when the wrinkled surface was located at the front side and full area around the square. It means the wrinkled surface can be optimized. An interesting point is that the drag coefficient was very similar between a model with front wrinkles and all sides wrinkles. Therefore, we know that the front side is quite important to reduce the drag force in fluid flow applications.

To determine the effects of Reynolds number, we conducted CFD analyses on three different base models, such as square, rhombus and circle. As shown Figs. 8(a)-(f), each model has with and without wrinkles on its surface (the width

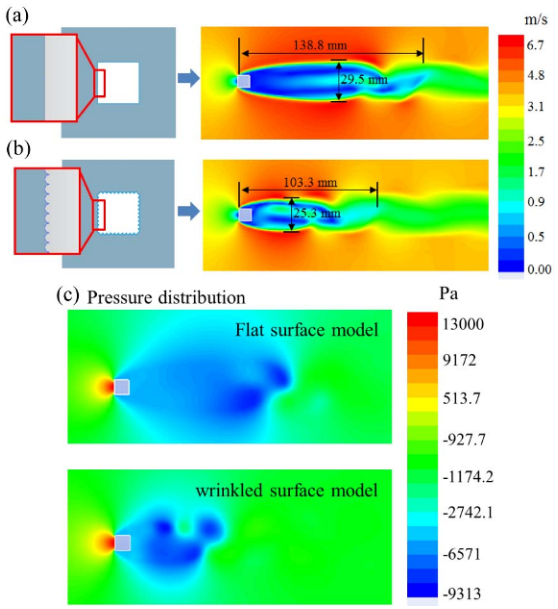

Fig. 5. Velocity contours of each model: (a) A flat square model; (b) a square with wrinkles; (c) comparison of pressure distributions.

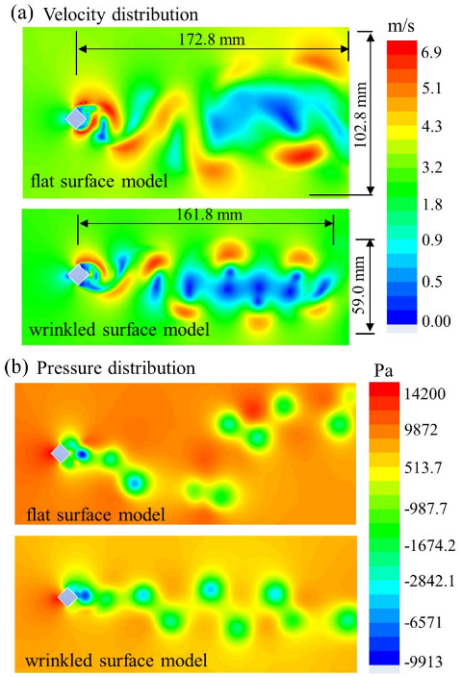

Fig. 6. Velocity contours of each model: (a) Flat rhombus model and rhombus with wrinkles; (b) comparison of pressure distributions.

of wrinkle was the same as previous one, 0.6 mm). The results show that the drag coefficient was reduced by increase of Reynolds number from 2000 to 50000 owing to increasing flow velocity.

3.2 Real 3D wrinkle model

From the analyses of simplified 2D wrinkled models, it is

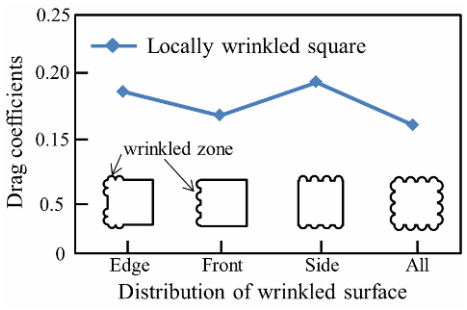

Fig. 7. Variation of a drag coefficient according to the location of wrinkled zone.

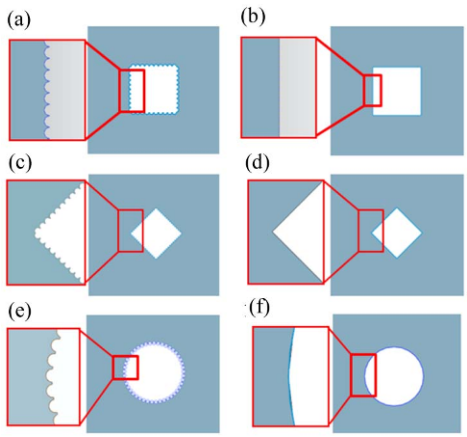

Fig. 8. Three types of analysis model: Square, rhombus, and circle with and without surface wrinkles.

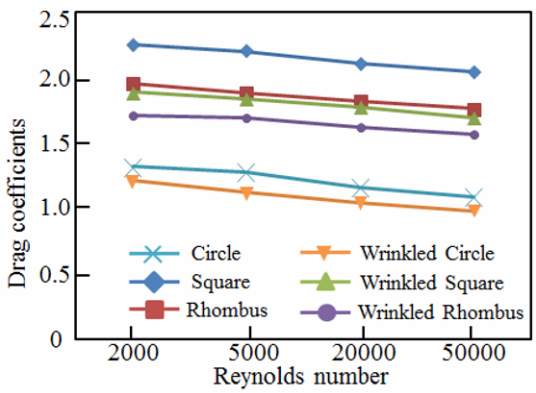

Fig. 9. Comparison of the variation of drag coefficient depending on Reynolds number.

obvious that the surface wrinkle is somewhat advantageous on reducing drag coefficient. Now, we tried to analyze a real 3D wrinkled surface to evaluate the effects on reduction of flow resistance. A real 3D wrinkling surface was modeled by the structural restoration of 3D scanned real fabricated wrinkles using MIMICS (Materialise, Belgium). However, there were some defects on a numerical model constructed by MIMICS due to scanning data errors. So, we modified the CAD data using a GEOMAGIC (3D systems, U.S.A.) (see Fig. 10(a)).

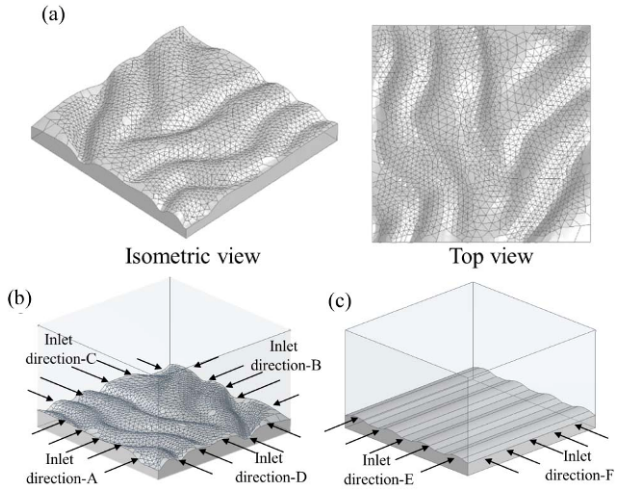

Fig. 10. (a) Final model of a scanned real 3D wrinkling surface and boundary condition of fluid field domain; (b) flow analysis of four directions on real wrinkles (direction-A to -D); (c) flow analysis of direction on modeled line wrinkles (direction-E and -F).

Average width of the 3D wrinkle model was 0.6 mm, and the average height was 0.1 mm. CFD analysis was performed using the real 3D wrinkled surface at the Re of 6000.

As shown in Figs. 10(b) and (c), the fluid field that was set at the inlet boundary of the 1.5 m/s velocity and the outlet boundary of the 0 Pa pressure was modeled. The grid layers were finely divided on around wrinkle structure using the inflation function. The fluid of water was used in CFD analysis at a temperature of 25 ℃. The size of the flow field domain was 3×3×2.5 mm. The standard k-ε was applied as a turbulence model, and the shape layers were finely divided using the inflation function. The grid dependency test was performed and the number of grids converged at the element number of 12×10^5.

To analyze the variation of drag coefficient according to four flow directions over the wrinkle surface, six cases were modeled (see Figs. 10(b) and (c)). From the CFD analyses, fluid flow characteristics were analyzed by comparing the flat surface and wrinkled surface according to different flow directions. In Figs. 11(a)-(f), the velocity contours with streamlines were depicted.

Under the Re of 6000, the drag coefficient of direction-A was 0.238, the direction-B was 0.241, the direction-C was 0.229, and the direction-D on the real wrinkling surface was 0.231. Also, the drag coefficient of direction-E was 0.230, and the direction-F on a line shaped wrinkles was 0.223 (see Fig. 12). In case of the real 3D wrinkle model, the variation of drag coefficient according to four flow directions was not much, less than 5 % difference. Also, the straight line shaped wrinkle showed somewhat better effects on the reduction of drag coefficient. So, further study needs to fabricate directionally controlled surface wrinkles. However, the direction-C has a similar flow direction to the direction-E of the line wrinkles, and two cases show the best result among others. Compared to

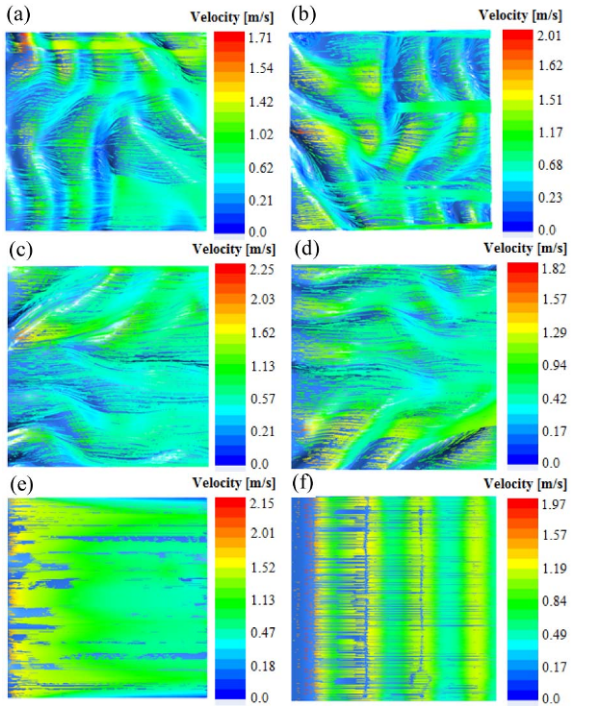

Fig. 11. Analysis results according to flow directions at Reynolds number of 6000; (a) Direction-A; (b) direction-B; (c) direction-C; (d) direction-D on the real wrinkle surface; (e) direction-E; (f) direction-F on a line wrinkle surface.

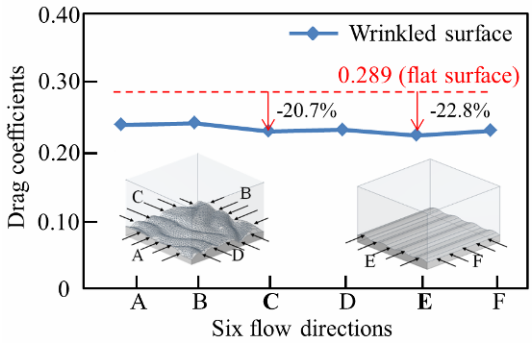

Fig. 12. Comparison of drag coefficients according to six flow directions on a real 3D wrinkle surface and a line shaped 3D wrinkle one.

that of a flat surface, the drag coefficients were reduced to 20.7 % and 22.8 %, respectively. The reason is average flow velocity of two cases (direction-C and -E) is higher than other cases. So, the drag coefficients of two cases became lower (see Eq. (1) and Fig. 12).

CFD results showed that the drag coefficient of the wrinkled shapes was at least 17.1 % lower than that of a flat surface. We believe that there are two factors to reduce a drag coefficient. One is a small low pressure zone of wake which induces to reduce the pressure difference between the front and rear of an object; therefore, the drag force (F_d) can be also minimized. The other is a vortex generation between wrinkles that leads a local slip condition of fluid flow. By that reason,

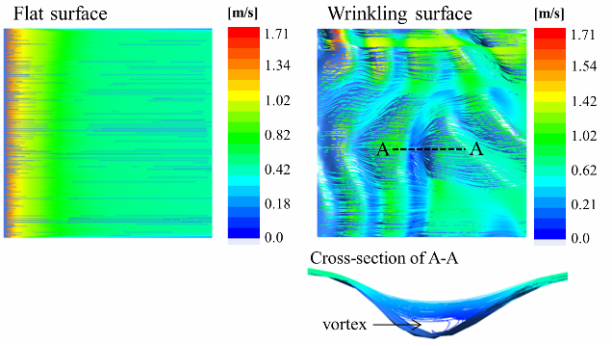

Fig. 13. Comparison of velocity profiles between a flat surface (left) and a wrinkling surface (right). Cross section of A-A shows a vortex generation between wrinkles.

the flow velocity becomes increased under a wrinkled surface (see Fig. 13).

4. Conclusions

We analyzed the effects of surface wrinkles using 2D and 3D models. Based on the fabrication results of metallic wrinkles, the fluid flow analysis of 2D and 3D model was built up for realizing the size of surface wrinkles. When the Reynolds number was 20000, the 2D square model with wrinkles reduced the flow resistance about 17.1 % due to a small amount of pressure difference between the front and rear side of the square. Also, the drag coefficient was decreased by increase of Reynolds number in all cases.

By using a real 3D wrinkle model which was scanned from fabricated metallic wrinkles, we understood the reason why wrinkled surface had an effect on reducing a drag force. Also, the drag coefficient was reduced as 20.7 % according to flow direction-C owing to relative high flow velocity. From this work, we believe that a wrinkling surface can be fabricated easily and cheaply, and the surface has much potential possibilities to be utilized in diverse flow-related research fields.

Acknowledgments

This research was supported by Basic Science Research Pgram through the National Research Foundation of Korea (NRF) (No. 2017R1D1A1A09000923), and also partially supported by Human Resources Program in Energy Technology of KETEP, Korea (No.20164010201000).

References

[1] D. W. Bechert, M. Bruse and W. Hage, Experiments with three-dimensional riblets as an idealized model of shark skin, *Experiments in Fluids*, 28 (2000) 403-412.

[2] B. N. J. Persson, Wet adhesion with application to tree frog adhesive toe pads and tires, *Journal of Physics: Condensed Matter*, 19 (2007) 1-16.

[3] G. M. Whitesides, The origins and the future of microfluidics, *Nature*, 442 (2006) 368-373.

[4] D. Y. Zhang, Y. H. Luo, L. I. Xiang and H. W. Chen, Numerical simulation and experimental study of drag-reducing surface of a real shark skin, *J. of Hydrodynamics*, 23 (2011) 204-211.

[5] M. Ibn Eihaj and M. Schadt, Optical polymer thin films with isotropic and anisotropic nano-corrugated surface topologies, *Nature*, 410 (2001) 796-799.

[6] U. Manna, C. D. C. Matthew and M. L. David, Shrink-to-fit superhydrophobicity: Thermally-induced microscale wrinkling of thin hydrophobic multilayers fabricated on flexible shrink-wrap substrates, *Advanced Materials*, 25 (2013) 3085-3089.

[7] Y. Li, S. Dai, J. John and K. R. Carter, Superhydrophobic surfaces from hierarchically structured wrinkled polymers, *Applied Materials Interfaces*, 5 (2013) 11066-11073.

[8] Z. J. Zhao, X. Li and S. H. Park, Generation of various wrinkle shapes on single surface by controlling thickness of weakly polymerized layer, *Material Letters*, 155 (2015) 125-129.

[9] S. J. Kim, H. J. Park, J. C. Lee, S. Park, P. Ireland and S. H. Park, A simple method to generate hierarchical nanoscale structures on microwrinkles for hydrophobic applications, *Material Letters*, 105 (2013) 50-53.

[10] F. Greco, A. Bellacicca, M. Gemmi, V. Cappello, V. Mattoli and P. Milani, Conducting shrinkable nanocomposite based on au-nanoparticle implanted plastic sheet: Tunable thermally induced surface wrinkling, *ACS Applied Materials & Interfaces*, 7 (2015) 7060-7065.

[11] M. Guvendiren, S. Yang and J. A. Burdick, Swelling-induced surface patterns in hydrogels with gradient crosslinking density, *Advanced Functional Materials*, 19 (2009) 3038-3045.

[12] M. W. Moon, S. H. Lee, J. Y. Sun, K. H. Oh, A. Vaziri and J. W. Hutchinson, Controlled formation of nanoscale wrinkling patterns on polymers using focused ion beam, *Scripta Materialia*, 57 (2007) 747-750.

[13] Y. Xia and G. M. Whitesides, Soft lithography, *Angewandte Chemie International Edition*, 37 (1998) 550-575.

[14] T. Chuang, P. J. Hai, Y. Z. Chuan and H. L. Cong, Controlled fabrication of hierarchically microstructured surfaces via surface wrinkling combined with template replication, *Chinese Chemical Letters*, 26 (2015) 15-20.

[15] T. W. Lim and D. Y. Yang, Direct fabrication of nano-wrinkled 3D microstructures using fitfully accumulated two-photon polymerization, *Int. J. Prec. Eng. Manuf.*, 16 (2015) 2427-2431.

[16] S. M. Kang, J. H. Kim and S. M. Kim, Partial wrinkle generation for switchable attachment and high adhesion hysteresis, *Int. J. Prec. Eng. Manuf.*, 18 (2017) 133-137.

[17] X. Li, Z. J. Zhao and S. H. Park, Out-of-plane stretching for simultaneous generation of different morphological wrinkles on a soft matter, *Applied Physics A*, 122 (2016) 1-8.

[18] D. Y. Zhang, Y. H. Luo, L. I. Xiang and H. W. Chen, Nu-

merical simulation and experimental study of drag-reducing surface of a real shark skin, *J. of Hydrodynamics Ser. B*, 23 (2011) 204-211.

[19] F. E. Fish, P. W. Weber, M. M. Murray and L. E. Howle, The tubercles on humpback whales' flippers: application of bio-inspired technology, *Integrative and Comparative Biology*, 51 (2011) 203-213.

[20] J. Choi, W. P. Jeon and H. Choi, Mechanism of drag reduction by dimples on a sphere, *Physics of Fluids*, 18 (2006) 1-4.

[21] M. Kim, S. M. Lee, S. J. Lee, Y. W. Kim, L. Li and D. W. Lee, Effect on friction reduction of micro/nano hierarchical patterns on sapphire wafers, *Int. J. Prec. Manuf. Green Technol.*, 4 (2017) 27-35.

[22] D. H. Yu and A. Kareem, Numerical simulation of flow around rectangular prism, *J. of Wind Engineering & Industrial Aerodynamics*, 67 (1997) 195-208.

[23] J. Rodriguez-Hernandez, Wrinkled interfaces: Taking advantage of surface instabilities to pattern polymer surfaces, *Progress in Polymer Science*, 42 (2015) 1-41.

[24] B. A. Younis and V. P. Przulj, Computation of turbulent vortex shedding, *Computational Mechanics*, 37 (2006) 408-425.

[25] J. A. McGeough, M. C. Leu, K. P. Rajurkar, A. K. M. De Silva and Q. Liu, Electroforming process and application to micro/macro manufacturing, *CIRP Annals - Manufacturing Technology*, 50 (2001) 499-514.

[26] F. A. Chudnovskii, L. L. Odynets, A. L. Pergament and G. B. Stefanovich, Electroforming process and application to micro/macro manufacturing, *J. of Solid State Chemistry*, 122 (1996) 95-99.

[27] Y. Joshua, M. Feng, D. T. Matthew, A. A. O. Douglas, R. S. Duncan, N. L. Chun and W. Stanley, The mechanism of electroforming of metal oxide memristive switches, *Nanotechnology*, 20 (2009) 215201-215209.

Jeong Ho Yang is a M.S. course student at Pusan National University. His research interests are fabrication of microscale wrinkle and its application to fluidic flow characteristics.

Sang Hu Park is a Professor in the School of Mechanical Engineering at Pusan National University. He earned his M.A. and Ph.D. in mechanical engineering at Korea Advanced Institute of Science and Technology (KAIST, Korea) in 1996 and 2006, respectively. His research fields are the development of 3D printing process, mechanical design, and manufacturing technology, especially for multi-scale structures.